A. Capannolo, M. Lavagna
Adaptive State-Dependent Riccati Equation Control for Formation Reconfiguration in Cislunar Space
Journal of Guidance Control and Dynamics, In press - Published online 03/01/2022
doi:10.2514/1.G006540

Adaptive State Dependent Riccati Equation Control for Formation Reconfiguration in Cislunar Space

Andrea Capannolo * and Michèle Lavagna †
Polytechnic University of Milan, Milan, Italy, 20156

I. Introduction

DISTRIBUTED space systems represent a state-of-the-art approach to both ordinary and innovative mission objectives. The exploitation of multiple spacecraft distributed in space results in improved performance, with reduced expenditures on hardware. Several mission concepts, leveraging satellites in formation, have been developed or are currently under study for both Earth and space applications [1]. Applications span from triangulation of celestial events [2, 3], to the observation of Earth surface [4] as well as deep-space objects [5]. During the last two decades, formation flying concepts have also been explored in multibody dynamical environment [6–12] to enable new approaches to space missions, from asteroids exploration and exoplanets observation [13–16] to future manned Lunar and Martian exploration [17]. In particular, the exploration of Moon and Mars will be facilitated through an outpost, named "Lunar Gateway", located on a Nearly Rectilinear Halo Orbit (NRHO) around the Moon. The Gateway will be subjected to multiple rendezvous and dockings, thus making the planning and control of relative motion around it of the utmost importance.

In this context, it is desirable to have a system as autonomous as possible, capable of efficiently computing the required control actions through the on-board hardware, and with minimal amount of externally provided data. Furthermore, it is fundamental, as in many space applications, to design a scheme that minimizes the cost of the maneuvers. Also, the system shall be able to perform such tasks while coping with the nonlinear cislunar environment, and with the large distances from the Gateway and from the target points. These requirements pose tight constraints in the choice of a suitable control scheme. In particular, methods that rely on a global linearization of the dynamics, such as the *Linear Quadratic Regulator* (LQR) [18], or on linearized quantities around a target orbit, like the *Floquet theory-based control* [19], do not allow to deal with the large dynamics variations in distance and time in an effective way.Vice versa, schemes that rely on optimization in the nonlinear model, such as the *Model Predictive Control* (MPC) [20], provide very good results but impose a large computational burden to the hardware, and may not be suitable for on-board implementation. *Sliding mode control* allows to deal with nonlinear dynamics in a computationally lighter way and with good robustness properties [21]; however, such technique does not embed the concept of cost minimization, inevitably leading to transfer costs which could be further lowered if a different strategy was used. A good approach in

*Ph.D. Candidate, Aerospace Science and Technology Department, Via La Masa 32.
†Associate Professor, Aerospace Science and Technology Department, Via La Masa 32

this direction is represented by the *Zero-Effort-Miss/Zero-Effort-Velocity* (*ZEM/ZEV*) scheme, which was demonstrated to work effectively for spacecraft formation control [22]. Nevertheless, the simple formulation of the ZEM/ZEM is fuel-optimal only in a uniform gravitational environment [23], and a lack of a parameter to tune does not provide degrees of freedom to search for minimum cost options in the gravitationally variable environment of the Earth-Moon binary system.

A good trade-off is represented by the *State Dependent Riccati Equation controller* (SDRE) [24], which approaches the optimality of the LQR while dealing with the nonlinear dynamics, and (differently from the ZEM/ZEV) possesses weights that can be tuned according to the designer necessities (cost efficiency and target tracking effectiveness). A simple way of employing a SDRE controller is to use fixed weights, and tune or optimize their value for a specific scenario, to obtain the desired performance [25]. Further improvements can still be attained with fixed weight matrices, by modifying either the cost function, the Riccati equation, or by post-processing the controller output, to improve stability, costs, and computational efficiency [26]. Modifications in the cost function can also be introduced to deal with nonlinear formulations of the control terms, as done in [27]. An alternative method for improving the SDRE performance is to introduce variable weights, that adapt to the states at each time step [28]. The adaptation allows to apply the same control scheme for different scenarios, with only a single initial tuning of the parameters.

Because of this higher level of generality of the adaptive weights approach, the present paper explores the effectiveness of this strategy in the specific scenario of a spacecraft orbiting around the Lunar Gateway on a NRHO, characterized by large and sudden changes in the dynamics. The weights adaptation law is here designed to withstand the large variations in relative distance and speed between the spacecraft and the Gateway, while mitigating control effort and costs. Furthermore, time is embedded in the law to enable control over the transfer time regardless of the infinite-horizon formulation of the SDRE. To make the scenario more realistic, a discrete SDRE controller (for on-board implementation) is assumed, and computations are performed for the Orion spacecraft, with coherent mass and thrust, and using on-off actuators. The performance improvements given by the adaptive weights approach are highlighted through a comparison with a optimized, fixed weights scheme. Also, the scheme is compared to offline-optimized transfers, to show the limited increase in costs when adopting the on-board controller.

The paper is structured as follows. Section II introduces the preliminaries required for the understanding of the controller implementation and tests. First, it describes the dynamics employed for the analyzes, then it provides information about the guidance and the computation of the target point for the reconfiguration transfers. The actual design of the controller, and the mathematics behind it, are developed in Section III, where the adaptation law is introduced. Section IV describes the simulations carried out to assess the performance of the schemes, and their results. Finally, Section V draws the conclusions of this work, and suggests some critical points for future developments and evaluations.

II. Dynamical Scenario and Guidance Strategy

The section introduces the dynamical framework in which the control scheme is tested, and describes the guidance scheme for the reconfiguration maneuvers, to generate the target state to be tracked by the controller.

A. CRTBP Dynamics

The dynamics of the CRTBP represent a simplification of the complex motion of an object around a binary system. The major simplification consists of assuming that the two massive attractors of the binary system are orbiting around each other at a constant distance (i.e. with circular motion), and that the third mass is small enough not to affect the other objects. Furthermore, the equations are expressed in a non-inertial reference frame, which rotates along with the attractors. This makes the system autonomous [29], and approximated periodic solutions can be easily found. The autonomous nature of the problem allows to define a pseudo-potential function, which reads:

$$U = \frac{1}{2}(x^2 + y^2) + \frac{1-\mu}{r_1} + \frac{\mu}{r_2} \tag{1}$$

with $\mu = \frac{m_2}{m_1+m_2}$ being the ratio between the secondary (smaller) attractor of the binary system, and the overall system's mass, and r_1 and r_2 being the third object's distance from the primary and secondary attractors respectively.

The equations of motion then read:

$$\begin{aligned} \ddot{x} - 2\dot{y} &= U_x \\ \ddot{y} + 2\dot{x} &= U_y \\ \ddot{z} &= U_z \end{aligned} \tag{2}$$

with $\dot{(\cdot)}$ and $\ddot{(\cdot)}$ being the first and second time derivatives of the state, and the subscripts x,y,z denoting the partial derivatives of the pseudo-potential function with respect to the position the spacecraft.

All presented quantities are computed in non-dimensional units, by setting:

$$\begin{aligned} m_1 + m_2 &= 1 \\ L &= 1 \\ \Omega = \sqrt{\frac{G(m_1+m_2)}{L^3}} &= 1 \end{aligned} \tag{3}$$

where L is the distance between the two attractors, Ω is the rotation rate of the binary system, and G is the gravitational constant.

B. Guidance scheme

The reconfiguration maneuvers are designed such that the chaser remains in the surroundings of the target spacecraft before, during, and after the transfer, hence avoiding drift motions along the reference NRHO orbit. To do so, the guidance scheme always aims at natural bounded motions around the target. This is here obtained by leveraging quasi-periodic invariant tori (*QP-tori*) around periodic orbits in CRTBP [30–32]. Such surfaces define the subspace of natural quasi-periodic orbits around a reference, periodic trajectory, suitable to maintain a spacecraft in formation at virtually null station-keeping costs. While multiple QP-tori may exist around a periodic orbit [33], the subset having the same orbital period as the reference periodic orbit is here selected, to avoid natural relative drifts along the reference trajectory. The subset is obtained through a *correction-continuation* numerical scheme [34], where the orbital frequency is enforced in the correction process. In particular, each torus must satisfy the following equations:

$$D^{-1}R(\rho)D\mathbf{X}_f - \mathbf{X}_i = \mathbf{0} \tag{4}$$

$$< \mathbf{X}_i - \tilde{\mathbf{X}}_i, \frac{\partial \tilde{\mathbf{X}}_i}{\partial \theta_0} > = 0 \tag{5}$$

$$< \mathbf{X}_i, \frac{\partial \tilde{\mathbf{X}}_i}{\partial \theta_1} > = 0 \tag{6}$$

$$\tau - \tau_p = 0 \tag{7}$$

Here, Eq. 4 imposes that the final states (after one orbital period) belong to the same stroboscopic map of the initial states, and that they are rotated along the map of an angle $\rho = 2\pi\frac{\omega_0}{\omega_1}$, with ω_0 and ω_1 being the two frequencies of the torus. Equations 5 and 6 are the *Phase Conditions*, ensuring anchoring of the stroboscopic map along the two dimensions of the torus. Finally, Eq. 7 verifies that the torus maintains the same period of the reference periodic orbit.

The output is a grid of states defining the torus, associated with a *longitude* angle (θ_0) and a *phase* angle (θ_1). The longitude angle defines the local stroboscopic map of the torus (i.e. the locus of possible natural states at a fixed time around the main spacecraft), while the phase angle describes the specific state on the local stroboscopic map. Figure 1 depicts an example of a large torus around a NRHO, with a sample of a quasi-periodic trajectory (fixed phase, variable longitude) and a series of stroboscopic maps (fixed longitude, variable phase). Notice that the quasi-periodic trajectory has a discontinuity on the stroboscopic map at the apolune; the phase difference between the initial and arrival points on the stroboscopic map is the rotation angle ρ. Then, the target state for the reconfiguration can be computed from the interpolation of the states grid, as a function of the time-varying longitude and phase angles, as:

$$\mathbf{x_T} = \mathbf{s}(\theta_0(t_0) + \omega_0(t - t_0), \theta_1(t_0) + \omega_1(t - t_0)) \tag{8}$$

with $\mathbf{s}$ being the interpolating vector-valued function. Notice that, while the phase θ_1 drives the reconfiguration, the

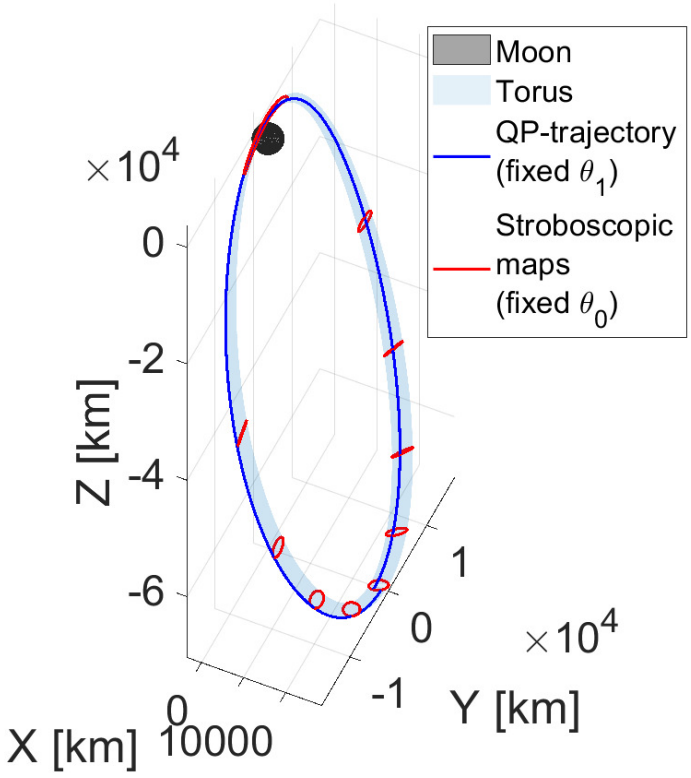

Fig. 1 Representation of stroboscopic maps and quasi-periodic trajectory on a QP-Torus.

longitude θ_0 of the target point must be equal to the one of the main spacecraft along the reference orbit, to maintain the formation also during the reconfiguration process.

III. SDRE Controller Design

The section introduces the mathematical formulation of the control scheme, and describes the strategy for the tuning of the controller's weights.

A. SDRE Formulation

The general formulation of the infinite-horizon SDRE control resembles the one of the classical Linear Quadratic Regulator (*LQR*) [35], which is sequentially applied to local linearization of the nonlinear dynamics. Given the nonlinear system

$$\dot{\mathbf{x}} = \mathbf{f}(\mathbf{x}) + \mathbf{g}(\mathbf{x}) \tag{9}$$

being $\mathbf{f}(\mathbf{x})$ the free-dynamics terms, and $\mathbf{g}(\mathbf{x})$ the active control terms, the linearization returns

$$\dot{\mathbf{x}} = A(\mathbf{x})\mathbf{x} + B(\mathbf{x})\mathbf{u} \tag{10}$$

with $\mathbf{u}$ the active control vector. The design of the standard SDRE control law for the system of Eq. 10 aims at computing the gain $K(\mathbf{x})$ such that

$$\mathbf{u} = -K(\mathbf{x})\mathbf{x} \tag{11}$$

In order for the SDRE to work, the K matrix has to be computed at each time step, and A and B matrices are to be updated accordingly. From the definition of the state-control dependent cost function, in the form

$$J = \int_0^\infty \left(\mathbf{x}^\top Q(\mathbf{x})\mathbf{x} + \mathbf{u}^\top R(\mathbf{x})\mathbf{u} + 2\mathbf{x}^\top N(\mathbf{x})\mathbf{u}\right) dt \tag{12}$$

with Q,R and N being the weight matrices, the minimization problem leads to the system of equations returning the gain matrix:

$$A(\mathbf{x})^\top P(\mathbf{x}) + P(\mathbf{x})A(\mathbf{x}) - \big(P(\mathbf{x})B(\mathbf{x}) + N(\mathbf{x})\big)R(\mathbf{x})^{-1}\big(B(\mathbf{x})^\top P(\mathbf{x}) + N(\mathbf{x})^\top\big) + Q(\mathbf{x}) = 0 \tag{13}$$

$$K(\mathbf{x}) = R(\mathbf{x})^{-1}\big(B(\mathbf{x})^\top P(\mathbf{x}) + N(\mathbf{x})^\top\big) \tag{14}$$

where Eq. 13 is the *Algebraic Riccati Equation* (ARE).

The scheme is then tailored to the analyzed problem. In particular, the formation reconfiguration problem is expressed as a *reference tracking* problem [36, 37], with completely decoupled state and control terms of the cost function. Furthermore, a discrete update of control actions is foreseen, to approximate a realistic behavior of a platform's hardware. A sampling time T_s is set as interval between one control action and the next one. The continuous dynamics of Eq. 10 becomes [38]

$$\begin{aligned} \mathbf{x}_{k+1} &= A_d(\mathbf{x}_k)\mathbf{x}_k + B_d(\mathbf{x}_k)\mathbf{u}_k \\ A_d &= e^{AT_s} \\ B_d &= \int_0^{T_s} e^{A\tau} B \, d\tau \end{aligned} \tag{15}$$

with k indicating the current time instant.

Then the final formulation of the discrete, reference tracking SDRE reads [39]

$$J_d = \sum_{k=0}^{\infty} (\mathbf{x}_k - \mathbf{x}_T)^\top Q(\mathbf{x}_k)(\mathbf{x}_k - \mathbf{x}_T) + \mathbf{u}_k^\top R(\mathbf{x}_k)\mathbf{u}_k \tag{16}$$

$$P_d = A_d^\top P_d A_d - \left(A_d^\top P_d A_d\right)\left(R + B_d^\top P_d B_d\right)^{-1}\left(B_d^\top P_d A_d\right) + Q \tag{17}$$

$$K_d = \left(R + B_d^\top P_d B_d\right)^{-1} B_d^\top P_d A_d \tag{18}$$

$$u_k = -K_d(\mathbf{x}_k - \mathbf{x}_T) \tag{19}$$

where Eq. 17 represents the *Discrete Algebraic Riccati Equation* (*DARE*). Notice that no target control action (u_T) is foreseen, as the target points subspace, defined in Section II.B, is characterized by natural trajectories in the CRTBP dynamics.

B. Weights tuning

Equations from Section III.A require the design and tuning of the weights $Q(\mathbf{x_k})$ and $R(\mathbf{x_k})$. In the present work, an on-board adaptation of the weights is proposed, to improve the autonomy of the controller scheme, while maintaining low transfer cost, and ensuring the completion of the transfers within the available time, despite the infinite-horizon formulation of the controller. To provide a benchmark for the assessment of the adaptive weights controller performance, a standard approach is also explored, optimizing fixed weights values to ensure minimum cost transfers, within the allowed transfer time. The two strategies are described hereafter.

1. Fixed Weights

The setup of the *Fixed Weights* approach foresees a preliminary simplification of the Q and R arrays. Given the problem of minimizing the cost function J from Eq. 16, variations of the minimum are only affected by the ratio between the two weight matrices. Consequently, it is sufficient to fix R (as a 3×3 identity matrix), and optimize Q. To further reduce the number of optimization variables, a diagonal Q is here considered, with the 3 weights associated with positions, and the 3 associated with velocity equal among themselves. The two arrays read:

$$\begin{aligned} Q &= \begin{bmatrix} q_r I_3 & 0_3 \\ 0_3 & q_v I_3 \end{bmatrix} \\ R &= I_3 \end{aligned} \tag{20}$$

with q_r and q_v being the *positions weight* and *velocities weight* respectively.

The optimization problem acts on the two variables only, and it is formulated as follows:

$$\min_{q_r, q_v} \Delta V \quad s.t. \quad \Delta T \leq ToF \tag{21}$$

where the ΔV and the ΔT are the cumulative cost and total time measured at the end of the controlled transfer, when the spacecraft-target point displacement falls below a user-defined threshold Δr_T, and ToF is the maximum allowed *Time of Flight*.

2. Adaptive weights

The adaptive approach follows the same simplifications of the fixed weights approach, i.e. it fixes R as an identity matrix, and considers only diagonal terms for the Q matrix, organized in positions weight q_r and velocities weight q_v. Nevertheless, the weights are not directly optimized. In particular, the positions weight follows a law to adapt its value during the transfer:

$$q_r = \alpha^{\beta} q_{MAX} \tag{22}$$

Here, q_{MAX} is a user-defined value, ad indicates the maximum value allowed for the position components.

$\alpha = \alpha(\Delta r, \Delta r_T)$ is a coefficient function of the local distance from target point (Δr) and the maximum displacement allowed at the end of the transfer (Δr_T), and reads:

$$\alpha = \frac{\Delta r_T}{\Delta r} \tag{23}$$

The inverse proportionality between the target distance and the α coefficient allows to keep the position-related part of the cost function moderate when distances are large, and favor the minimization of such component only when transfer is almost completed. Notice that, by its expression, it is always greater than zero, but may exceed the unitary value if the distance is shorter than the maximum allowed displacement. This shall be avoided as a maximum weight value of q_{MAX} is desired, hence a saturation is applied.

$\beta = \beta(ToF, t, \Delta t_{exp})$ is the exponent of the parameter α, and depends on time-related parameters, namely the allowed ToF, the current time t, and the linearized expected time for convergence Δt_{exp}. The latter is a local approximation of the time required to reach the target, and is computed from the ratio between target distance and relative radial velocity:

$$\Delta t_{exp} = \frac{\Delta r}{\Delta \dot{r}} \tag{24}$$

The β exponent acts by reducing or increasing the α nominal value depending on the time left to complete the transfer. In particular, its expression reads:

$$\beta = 1 + \frac{ToF - t}{\Delta t_{exp}} \tag{25}$$

According to Eq. 25, β tends toward small values as t approaches ToF (the available time is running out) or as Δt_{exp} becomes large (the expected convergence time is too long). Small values of β make α^{β} approach the value of 1, thus maximizing the position weights and providing a more aggressive control. On the contrary, larger β values (with long time available or fast target approaching) scale α^{β} towards 0, making the control milder. Preliminary tests on the adaptation scheme showed that initial rough estimations on the convergence time Δt_{exp} may lead to large β jumps towards small values, which generate excessively prompt control responses and higher costs. To overcome this problem,

a limiter $\Delta\beta$ is set for β decrement only. Hence, Eq. 25 is modified into:

$$\beta = \max\left(\left[1 + \frac{ToF - t}{\Delta t_{exp}} \quad , \quad \beta_0 - \Delta\beta\right]\right) \tag{26}$$

Notice that this requires the storage, at each iteration, of the previous β value, namely β_0.

The full adaptation scheme is depicted in Figure 2.

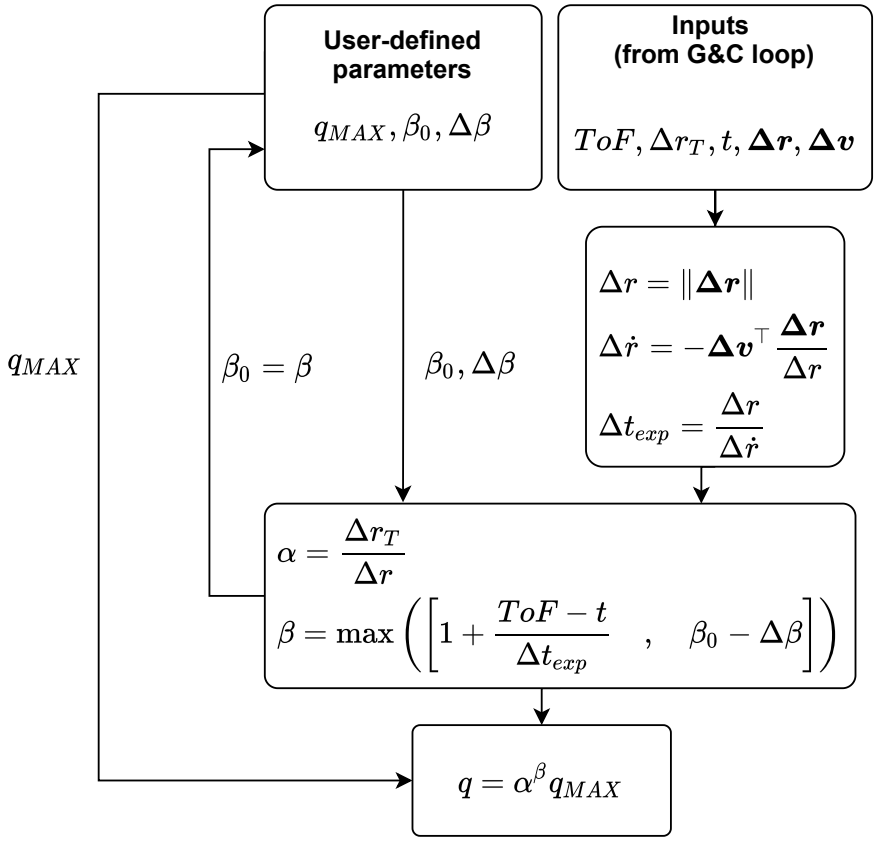

Fig. 2 Weights adaptation scheme

IV. Simulations and results

The section presents the result of the overall performance for the adaptive SDRE scheme. First, reference cost maps are developed through optimal impulsive transfers, to provide a reference for assessing the on-board controller performance. Then, the on-board controller in the *Fixed Weights* and *Adaptive Weights* forms are tested, and performance improvement with the weights adaptation analyzed.

A. Reference scenario and optimal costs

The reference trajectory is the NRHO designed to host the Lunar Gateway. It is a resonant orbit (9:2 Moon resonance), with a perilune above the Moon's north pole of approximately 3250 km and an apolune of 71 000 km, and an overall orbital period of 6.526 days [40]. The selected quasi-periodic torus around the NRHO is a medium-sized torus, with main characteristics reported in Table 1, and depicted in Figure 3. This choice has been made to highlight the

ρ $[deg/orbit]$	Avg. Dist $[km]$	Max. Dist. $[km]$	Min. Dist. $[km]$
46.9214	336.80	1824.10	102.33

Table 1 Rotation number, and average/maximum/minimum distance of the torus from the Gateway

difference in performance between the proposed scheme and the fixed weights SDRE. Nevertheless, the advantages of the adaptive weights scheme can be extended to smaller formations, as the torus structure is mostly preserved, although scaled in size.

Optimal transfers are computed to connect any point of the toroidal surface leveraging three impulsive maneuvers (with the middle one executed at the best time along the transfer to minimize costs), as reported in [41]. A limit on the maximum ToF is set to 48 h, compatibly to realistic operational times of the Gateway approach. Given the impulsive nature of the maneuvers here considered, no information about the platform (weight and thrust level) are required, and will be described in Section IV.B where the on-board scheme (which provides an acceleration input) is analyzed.

The full cost map, as a function of initial longitude (θ_{0i}), initial phase (θ_{1i}) and final phase (θ_{1f}) is depicted in Figure 4. From the map it is possible to identify layers of increasing cost, as inclined planes along the θ_{1i}/θ_{1f} bisector. Such planes correspond to the loci with constant phase change $\Delta\theta_1 = \theta_{1f} - \theta_{1i}$. In particular, maximum cost variation along both longitude and phase directions is observed for the plane at $\Delta\theta_1 = 180°$, depicted in Figure 5. Such phase variation corresponds to a complete,"from side to side" shift around the Gateway, thus requiring more effort to cover the larger distance between initial and target points within the available amount of time. The map highlights a variation of transfer costs from around 5 m s^{-1} to nearly 15 m s^{-1}, strongly affected by the phase and the longitude parameters (thanks to the geometry and symmetries of the toroidal surface). In particular, the perilune passage (corresponding to the longitude value of $\theta_{0i} = 180°$) demonstrated to be particularly critical, as it provides the most and the least expensive transfers, depending on the initial phase. Such 2D map is taken as reference to measure cost increments from the on-board control scheme, described in the next section.

B. On-Board Controller Performance

To analyze the performance of the SDRE controller, information about the platform are needed, as the control action acts as an acceleration through time. The Orion spacecraft is considered as a reference scenario, with a total (wet) mass

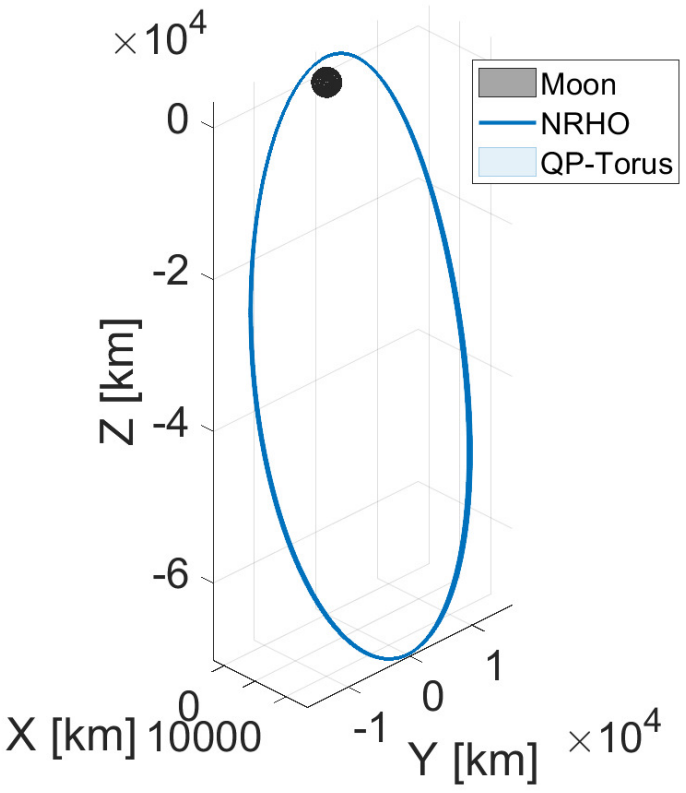

(a) View from Earth-Moon barycenter

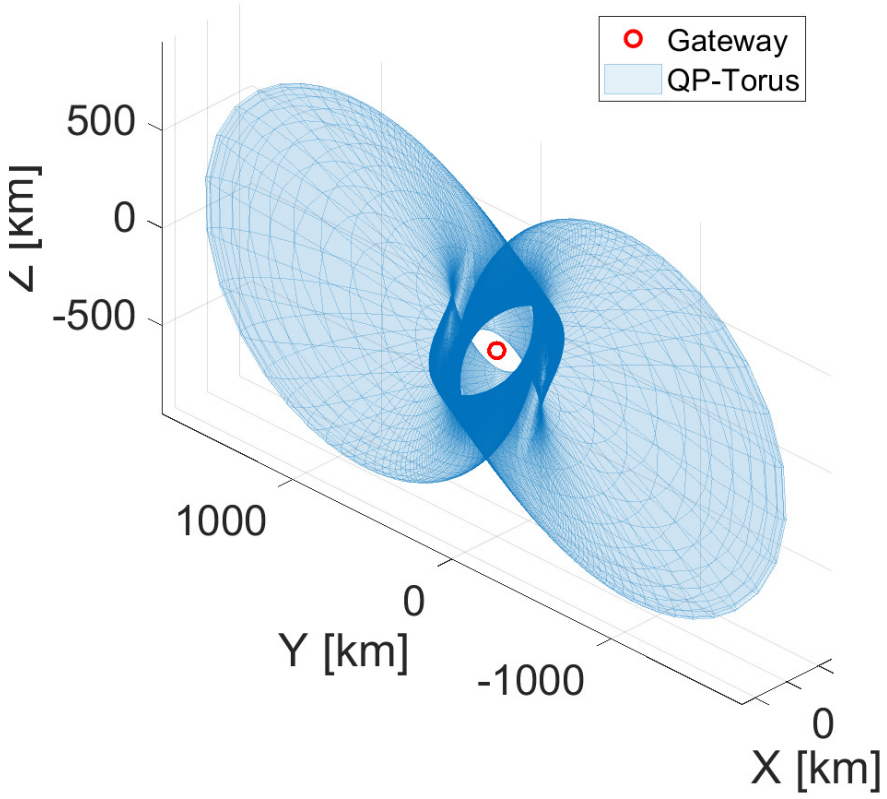

(b) View from Gateway

Fig. 3 Quasi-Periodic Torus in Earth-Moon rotating frame

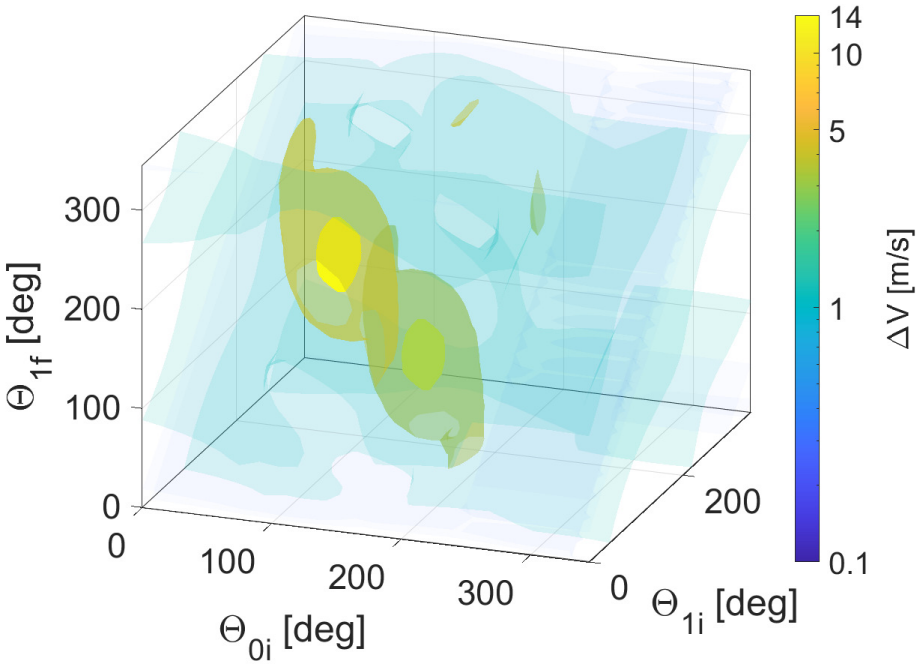

Fig. 4 3D cost map for optimal 3-impulses transfers

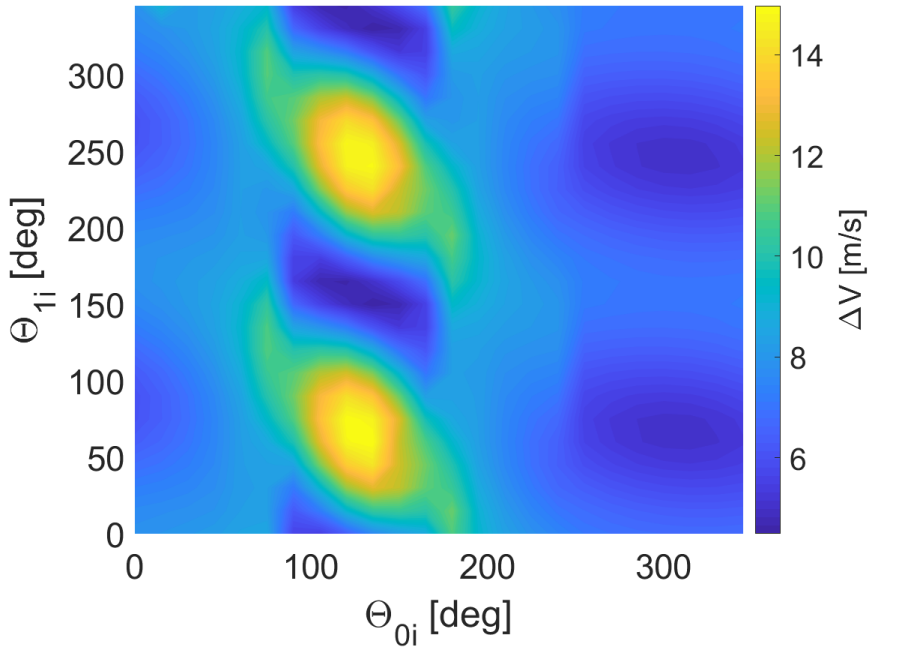

Fig. 5 Cost map as function of initial longitude and phase, for a phase change of 180°

of 25 855 kg. In the present analysis, only four of the eight 490 N auxiliary thruster are exploited for controlling the spacecraft, leading to a fixed acceleration of $0.0758\,\mathrm{m\,s^{-2}}$.

Given the fixed thrust nature of the platform, the variable input u provided by the controller is modified through a *Pulse-Width Modulation* (PWM). In particular, a sampling time $T_s = 600\,\mathrm{s}$ is considered, in which the output of the SDRE control assumes a continuous control action; the PWM takes the actual acceleration provided, and recomputes the new thrust time T_u needed to obtain the same ΔV, namely:

$$T_u = \frac{u}{\tilde{u}} T_s \tag{27}$$

with $\tilde{u}$ being the fixed acceleration provided by the platform, after non-dimensionalization according to the CR3BP parameters.

One last remark regards the high cost peak that affects both *Fixed Weights* and *Adaptive Weights* on-board control across the perilune passage, caused by very close proximity to the Moon and fast dynamics. Differently from the impulsive maneuvers of Section IV.A, the on-board controller provides control actions at each sampled time across the whole transfer, and it is not capable of optimizing the location of the maneuvers. This implies the presence of active control also when very close to the perilune, leading to the observed cost increment. To partially workaround this issue, shorter ToF are imposed to all transfers that would cross the perilune location, such that the transfers are always completed before the closest approach of the Moon. Although this approach leads to a cost increment, the very high cost peaks measured at perilune are significantly reduced.

1. Fixed weights

The *Fixed Weights* approach requires, as mentioned in Section III.B.1, a dedicated optimization for each transfer, i.e for each θ_{0i}/θ_{1i} couple. The result is a map of the position and velocity weights magnitude, as depicted in Figure 6. The first feature that stands out is the large increment of the weights magnitude at perilune ($\theta_{0i} = 180°$) of several orders of magnitude, necessary to withstand the faster natural dynamics. Secondly, a milder effect of the phase (θ_{1i}) is also observed, with approximately an order of magnitude reduction for the phases around $\theta_{1i} = 0°/180°$. This is justified by the shorter initial distance between initial and target points at such phase values, due to the shape of the stroboscopic maps along the torus.

With the computed weights maps, the corresponding cost map is developed (depicted in Figure 7). Overall higher costs with respect to the optimal-impulses transfer are observed, with an increase of $5\,\mathrm{m\,s^{-1}}$ at least (for the region nearby the apolune). This is mainly due to the discretized control actions across the whole transfer, which provide a suboptimal solution if compared to the optimized impulsive maneuvers. Cost oscillations with the phase are again justified by the distance variation between initial and target point along the stroboscopic maps, which particularly affect

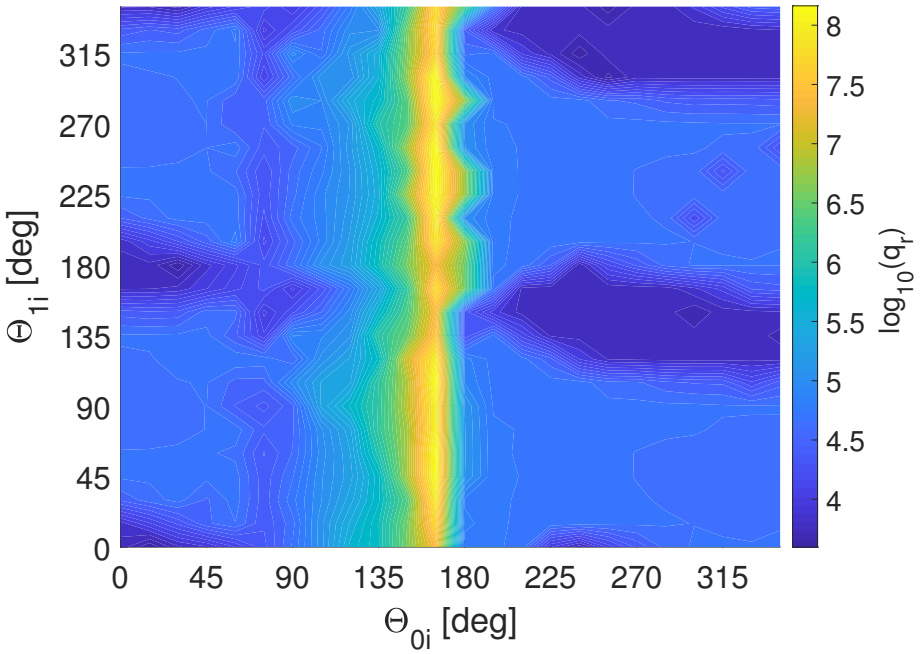

(a) Positions weight

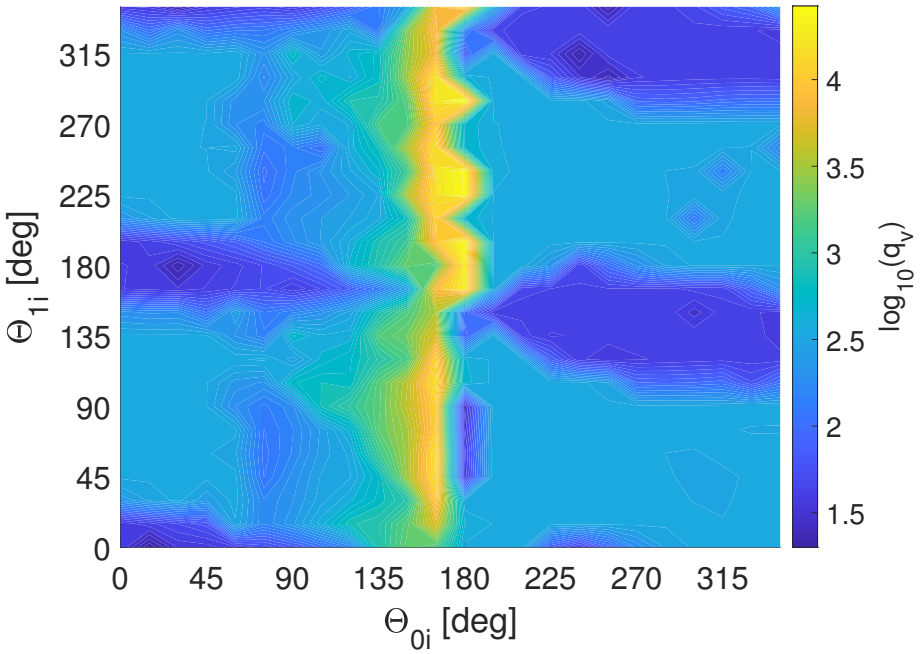

(b) Velocities weight

Fig. 6 Optimized weights for all the transfers in the *Fixed Weights* approach

this strategy as weights, despite their optimization, are fixed values and make the control action sensitive to the distance itself. Furthermore, the higher weights across the perilune region, despite ensuring the completion of the transfer, make the cost levels impractical for a real application, with a ΔV above $100\,\mathrm{m\,s^{-1}}$. In general, costs below $20\,\mathrm{m\,s^{-1}}$

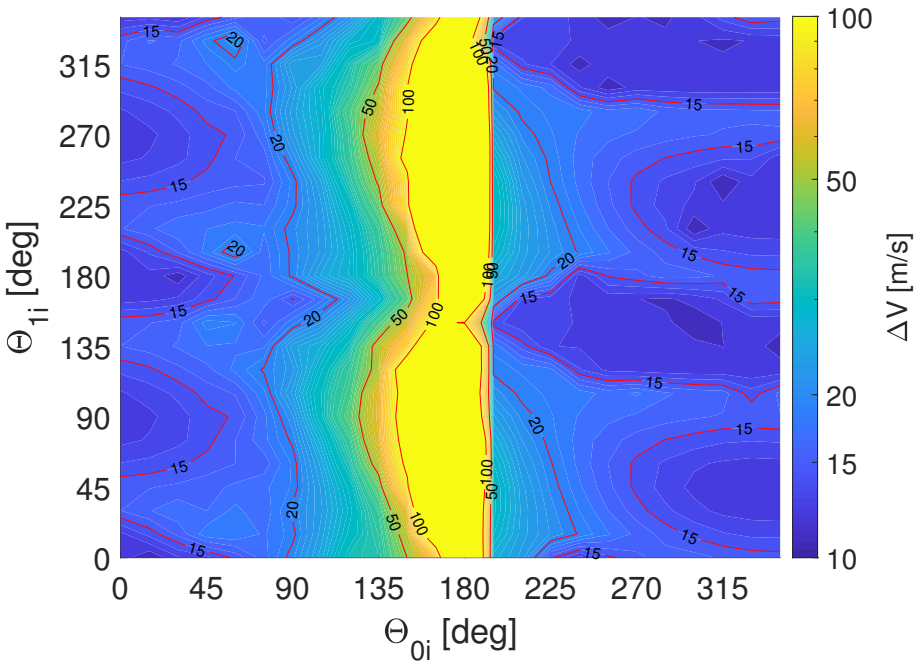

Fig. 7 Cost map for transfers with *Fixed Weights* approach

are observed for the torus regions of interest, where maneuvers are likely to be performed in a realistic scenario. This makes the on-board approach a suitable alternative to on-ground optimization and uplink of maneuvers, and provides a step towards a higher autonomy of the *Orion-Gateway formation*. Nevertheless, the offline optimization of the weights represents itself a downside of this approach, requiring it a computationally expensive tuning for the on-board controller.

2. Adaptive weights

The *Adaptive Weights* approach aims at overcoming the downsides of the *Fixed Weights* approach, i.e. the cost variation due to oscillations in the target state distance, and the intensive weights optimization for each transfer along the torus. The adaptation law (from Eq. 22), deals, by design, with the distance variation, and can be applied to any transfer without the need of a dedicated tuning. Nevertheless, a first tuning of the user-defined parameters (q_{MAX}, q_v, $\beta_0(t=0)$, $\Delta\beta$) is still required. The tuning process leads to the parameters' values listen in Table 2. With a single tuning of this four parameters, the *Adaptive Weights* SDRE controller provides the full cost map depicted in Figure 8. Here, a cost below $10\,\mathrm{m\,s^{-1}}$ (never reached in the *Fixed Weights* approach) can be observed for most of the torus regions, demonstrating the higher flexibility to distance variations. Indeed, the cost oscillations with respect to the phase are

q_{MAX} [−]	q_v [−]	$\beta_0(t=0)$ [−]	$\Delta\beta$ $[units/h]$
10^9	10^2	2	2

Table 2 Tuned parameters for the *Adaptive Weights* approach

nearly negligible, and a more uniform distribution is obtained. In general, for most regions of interest, it is observed a reduction of approximately $5\,\mathrm{m\,s^{-1}}$ with respect to the *Fixed Weights* approach. On the contrary, the region nearby

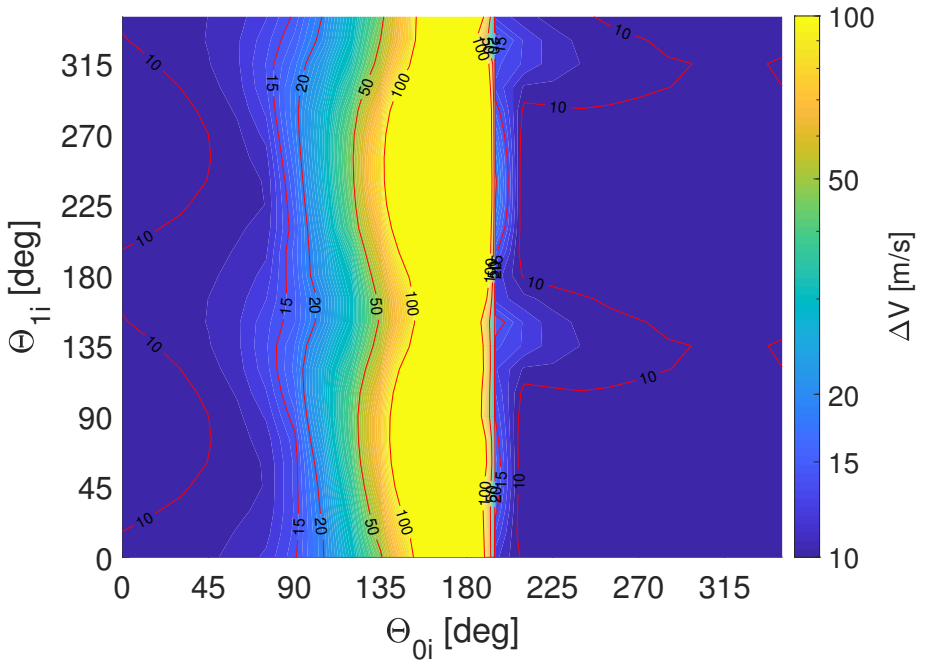

Fig. 8 Cost map for transfers with *Adaptive Weights* approach

the perilune appears to be comparable in terms of cost. Nevertheless, such result is here obtained without a dedicated optimization of such transfer, demonstrating the more general applicability of the *Adaptive Weights* approach.

To give more insight about the differences between the two approaches, a sample transfer, and corresponding costs, are depicted in Figure 9. The reference value of comparison is provided by the offline optimized transfer, which requires $8.2\,\mathrm{m\,s^{-1}}$ to reach the target phase/trajectory. The *Fixed Weights* SDRE, aiming at the stroboscopic map of each time instant, follows a deviated path along the transfer, leading to a higher cost ($17.3\,\mathrm{m\,s^{-1}}$). The *Adaptive Weights* controller, despite the same targeting philosophy, reacts to the low target-approaching velocity at the beginning of the transfer, and provides an initial higher control effort. After gaining speed and reducing the distance, the following of the target point demands less effort, thus leading to a visible cost reduction ($10.7\,\mathrm{m\,s^{-1}}$) and approaching the offline-optimal value.

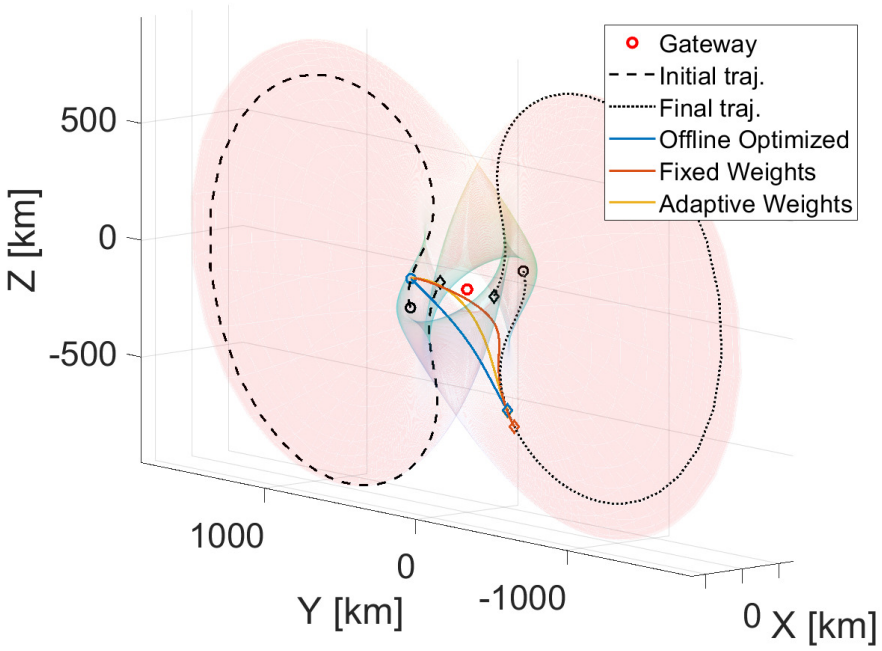

(a) 3D view of the transfer. Dashed and dotted black curves are the initial and final natural trajectories on the torus. Circle markers and diamond markers represent the beginning and the end of each curve respectively.

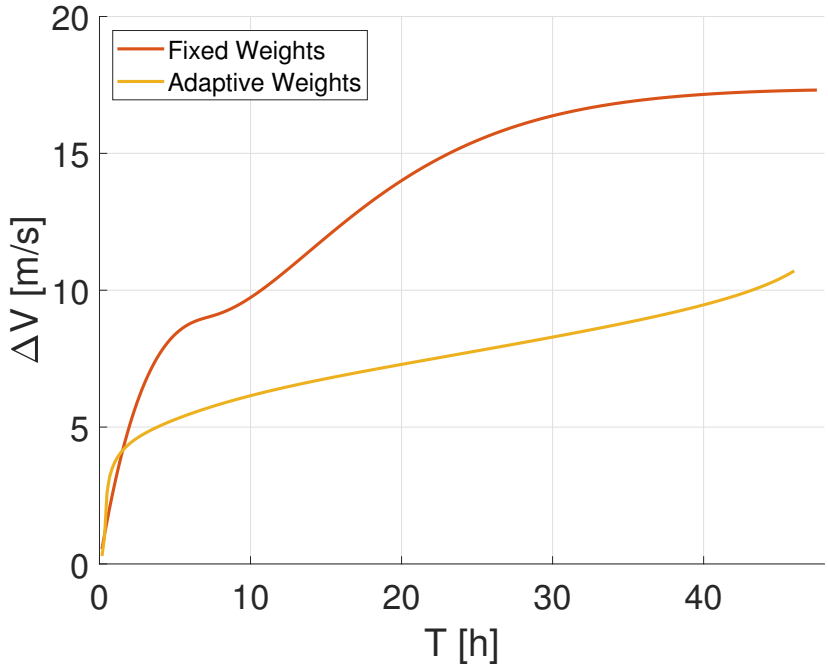

(b) Cumulative cost for the *Fixed Weights* and *Adaptive Weights* schemes.

Fig. 9 Transfer example for a phase shift from $45°$ **to** $225°$**, and from an initial longitude of** $60°$ **(branch of the torus approaching the Moon).**

V. Conclusions

The paper explored the topic of on-board controller design for performing reconfiguration of spacecraft formation, with a direct application to the Lunar Gateway-Orion spacecraft scenario. In particular, quasi-periodic trajectories around the NRHO (where the Gateway will be located) are explored as stationing surfaces to maintain the formation, and transfers from and to such surface are analyzed. The transfers are first developed through optimized, impulsive maneuvers to provide a reference cost map for a benchmark of the on-board controller performance. Then, the transfers are computed leveraging the SDRE controller, in the two cases with fixed, optimized weights of the cost function, and with variable weights according to an adaptation law.

In general, the on-board controller demonstrated to be capable of completing the transfer with an acceptable increase in costs with respect to the impulsive, optimal maneuvers case. The controller with fixed weights is also exploited to assess the advantages of using the adaptation law. Results highlighted an overall advantage of the latter over the former strategy. First, the adaptation law, despite a single initial tuning, proved its applicability in all regions of the torus, completing all transfers within the available amount of time. Secondly, its adaptation also in terms of distance from target state allowed to achieve lower costs than the fixed weights strategy, by making it less sensitive to initial natural distance between the start point and the target point along the torus.

The present study relied on the Circular Restricted Three-Body Problem as dynamics model, which inevitably leads to discrepancies from the actual Earth-Moon motions, and did not consider possible external perturbations such as the Solar Radiation Pressure. For this reason, the on-board SDRE controller shall be extended to a higher-fidelity dynamics, to assess its robustness in presence of unmodeled or unknown dynamics terms. In particular, an analysis on the region of attraction of the system, and on how it is affected by the uncertainties in the model, is required. Also, influence of the design parameters (spacecraft mass, thrust, time of flight) on the performance of the transfer shall be addressed. Finally, the adaptation law of the weights relies of parameters which have to be measured or estimated by the chaser spacecraft (Orion module) or provided by the main spacecraft (Lunar Gateway). This implies the inclusion of measurement/estimation errors within the control law, therefore such contributions shall be analyzed to verify the stability of the controller in presence of parameters' noise.

References

[1] Scharf, D., Hadaegh, F., and Ploen, S., "A survey of spacecraft formation flying guidance and control. Part II: control," *Proceedings of the 2004 American Control Conference*, Vol. 4, 2004, pp. 2976–2985 vol.4. https://doi.org/10.23919/ACC.2004.1384365.

[2] Colagrossi, A., Prinetto, J., Silvestrini, S., and Lavagna, M. R., "Sky visibility analysis for astrophysical data return maximization in HERMES constellation," *Journal of Astronomical Telescopes, Instruments, and Systems*, Vol. 6, No. 4, 2020, pp. 1 – 25. https://doi.org/10.1117/1.JATIS.6.4.048001.

[3] Scala, F., Zanotti, G., Curzel, S., Fetescu, M., Lunghi, P., Lavagna, M., and Bertacin, R., "The HERMES Mission: A CubeSat

Constellation For Multi-Messenger Astrophysics," *5th IAA Conference on University Satellite Missions and CubeSat Workshop*, 2020, pp. 1–17.

[4] Krieger, G., Moreira, A., Fiedler, H., Hajnsek, I., Werner, M., Younis, M., and Zink, M., "TanDEM-X: A Satellite Formation for High-Resolution SAR Interferometry," *IEEE Transactions on Geoscience and Remote Sensing*, Vol. 45, No. 11, 2007, pp. 3317–3341. https://doi.org/10.1109/TGRS.2007.900693.

[5] Kolmas, J., Banazadeh, P., Koenig, A. W., Macintosh, B., and D'Amico, S., "System design of a miniaturized distributed occulter/telescope for direct imaging of star vicinity," *2016 IEEE Aerospace Conference*, 2016, pp. 1–11. https://doi.org/10.1109/AERO.2016.7500783.

[6] Marchand, B. G., and Howell, K. C., "Control Strategies for Formation Flight In the Vicinity of the Libration Points," *Journal of Guidance, Control, and Dynamics*, Vol. 28, No. 6, 2005, pp. 1210–1219. https://doi.org/10.2514/1.11016.

[7] Scheeres, D., and Vinh, N., "Dynamics and control of relative motion in an unstable orbit," *Astrodynamics Specialist Conference*, 2000, p. 4135. https://doi.org/10.2514/6.2000-4135.

[8] Gurfil, P., and Kasdin, N., "Dynamics and control of spacecraft formation flying in three-body trajectories," *AIAA Guidance, Navigation, and Control Conference and Exhibit*, 2001, p. 4026. https://doi.org/10.2514/6.2001-4026.

[9] Folta, D., Carpenter, J. R., and Wagner, C., "Formation flying with decentralized control in libration point orbits," 2000.

[10] Colombi, F., Colagrossi, A., and Lavagna, M., "Characterisation of 6DOF natural and controlled relative dynamics in cislunar space," *Acta Astronautica*, 2021. https://doi.org/10.1016/j.actaastro.2021.01.017.

[11] Bando, M., and Ichikawa, A., "Formation Flying Along Halo Orbit of Circular-Restricted Three-Body Problem," *Journal of Guidance, Control, and Dynamics*, Vol. 38, No. 1, 2015, pp. 123–129. https://doi.org/10.2514/1.G000463.

[12] Ferrari, F., and Lavagna, M., "Formation flying and relative dynamics under the circular restricted three-body problem formulation," *Spaceflight Mechanics*, 2014, pp. 185–204.

[13] Seager, S., Kasdin, N. J., Booth, J., Greenhouse, M., Lisman, D., Macintosh, B., et al., "Starshade Rendezvous Probe Mission," *Bulletin of the AAS*, Vol. 51, No. 7, 2019.

[14] Farres Basiana, A., and Webster, C. M., "Wide-Field Infrared Survey Telescope and Starshade Formation Flying Dynamics at Sun-Earth L2," *Proceedings of the 69th International Astronautical Congress*, 2018.

[15] Sears, D., Allen, C., Britt, D., Brownlee, D., Franzen, M., Gefert, L., Gorovan, S., Pieters, C., Preble, J., Scheeres, D., and Scott, E., "The Hera mission: multiple near-earth asteroid sample return," *Advances in Space Research*, Vol. 34, No. 11, 2004, pp. 2270–2275. https://doi.org/10.1016/j.asr.2003.05.059.

[16] Ferrari, F., Franzese, V., Pugliatti, M., Giordano, C., and Topputo, F., "Preliminary mission profile of Hera's Milani CubeSat," *Advances in Space Research*, Vol. 67, No. 6, 2021, pp. 2010–2029. https://doi.org/10.1016/j.asr.2020.12.034.

[17] Crusan, J. C., Smith, R. M., Craig, D. A., Caram, J. M., Guidi, J., Gates, M., Krezel, J. M., and Herrmann, N. B., "Deep space gateway concept: Extending human presence into cislunar space," *2018 IEEE Aerospace Conference*, 2018, pp. 1–10. https://doi.org/10.1109/AERO.2018.8396541.

[18] Anderson, B. D., and Moore, J. B., *Optimal control: linear quadratic methods*, Courier Corporation, 2007, Chap. 2.

[19] Montagnier, P., Spiteri, R. J., and Angeles, J., "The control of linear time-periodic systems using Floquet–Lyapunov theory," *International Journal of Control*, Vol. 77, No. 5, 2004, pp. 472–490. https://doi.org/10.1080/00207170410001667477.

[20] Camacho, E. F., and Alba, C. B., *Model predictive control*, Springer science & business media, 2013, Chap. 2.

[21] Lian, Y., Gómez, G., Masdemont, J. J., and Tang, G., "Station-keeping of real Earth–Moon libration point orbits using discrete-time sliding mode control," *Communications in Nonlinear Science and Numerical Simulation*, Vol. 19, No. 10, 2014, pp. 3792–3807. https://doi.org/10.1016/j.cnsns.2014.03.026.

[22] Furfaro, R., Topputo, F., Mueting, J. R., Casotto, S., and Simo, J., "Analysis and performance evaluation of ZEM/ZEV guidance and its sliding robustification for autonomous rendezvous in relative motion," *Proceedings of the 67th International Astronautical Congress*, 2016.

[23] Drozd, K. M., Furfaro, R., and Topputo, F., "Application of ZEM/ZEV guidance for closed-loop transfer in the Earth-Moon System," *2018 Space Flight Mechanics Meeting*, 2018.

[24] Çimen, T., "State-Dependent Riccati Equation (SDRE) Control: A Survey," *IFAC Proceedings Volumes*, Vol. 41, No. 2, 2008, pp. 3761–3775. https://doi.org/10.3182/20080706-5-KR-1001.00635.

[25] Marsola, T. C. L., da Silva Fernandes, S., and Balthazar, J. M., "Stationkeeping controllers for Earth–Moon L1 and L2 libration points halo orbits," *Journal of the Brazilian Society of Mechanical Sciences and Engineering*, Vol. 43, No. 7, 2021, p. 347. https://doi.org/10.1007/s40430-021-03071-9.

[26] Franzini, G., Tannous, M., and Innocenti, M., "Spacecraft relative motion control using the state-dependent Riccati equation technique," *10th International ESA Conference on Guidance, Navigation & Control Systems*, Vol. 29, 2017.

[27] Rouzegar, H., Khosravi, A., and Sarhadi, P., "Spacecraft formation flying control around L2 sun-earth libration point using on–off SDRE approach," *Advances in Space Research*, Vol. 67, No. 7, 2021, pp. 2172–2184. https://doi.org/10.1016/j.asr.2021.01.008.

[28] Souza, L. C., and Bigot, P., "An adaptive method with weight matrix as a function of the state to design the rotatory flexible system control law," *Mechanical Systems and Signal Processing*, Vol. 79, 2016, pp. 132–140. https://doi.org/10.1016/j.ymssp.2016.02.028, special Issue from ICEDyn 2015.

[29] Szebehely, V., *Theory of orbit: The restricted problem of three Bodies*, Elsevier, 2012, Chap. 1.

[30] Baresi, N., "Spacecraft formation flight on quasi-periodic invariant tori," Ph.D. thesis, University of Colorado at Boulder, 2017.

[31] Olikara, Z. P., and Howell, K. C., "Computation of quasi-periodic invariant tori in the restricted three-body problem," *AAS/AIAA Space Flight Mechanics Meeting*, 2010.

[32] Olikara, Z. P., and Scheeres, D. J., "Numerical method for computing quasi-periodic orbits and their stability in the restricted three-body problem," *Advances in the Astronautical Sciences*, Vol. 145, No. 911-930, 2012.

[33] Olikara, Z. P., "Computation of quasi-periodic tori and heteroclinic connections in astrodynamics using collocation techniques," Ph.D. thesis, University of Colorado at Boulder, 2016.

[34] Baresi, N., Olikara, Z. P., and Scheeres, D. J., "Fully numerical methods for continuing families of quasi-periodic invariant tori in astrodynamics," *The Journal of the Astronautical Sciences*, Vol. 65, No. 2, 2018, pp. 157–182. https://doi.org/10.1007/s40295-017-0124-6.

[35] Cloutier, J., "State-dependent Riccati equation techniques: an overview," *Proceedings of the 1997 American Control Conference*, Vol. 2, 1997, pp. 932–936 vol.2. https://doi.org/10.1109/ACC.1997.609663.

[36] Mannava, A., Balakrishnan, S. N., Tang, L., and Landers, R. G., "Optimal Tracking Control of Motion Systems," *IEEE Transactions on Control Systems Technology*, Vol. 20, No. 6, 2012, pp. 1548–1558. https://doi.org/10.1109/TCST.2011.2168608.

[37] Strano, S., and Terzo, M., "A SDRE-based tracking control for a hydraulic actuation system," *Mechanical Systems and Signal Processing*, Vol. 60-61, 2015, pp. 715–726. https://doi.org/10.1016/j.ymssp.2015.01.027.

[38] DeCarlo, R. A., *Linear systems: A state variable approach with numerical implementation*, Prentice-Hall, Inc., 1989, Chap. 1.

[39] Lewis, F. L., Vrabie, D., and Syrmos, V. L., *Optimal control*, John Wiley & Sons, 2012, Chap. 4.

[40] Davis, D. C., Boudad, K. K., Phillips, S. M., and Howell, K. C., "Disposal, deployment, and debris in near rectilinear halo orbits," *29th AAS/AIAA Space Flight Mechanics Meeting*, 2019.

[41] Capannolo, A., and Lavagna, M., "Minimum Cost Relative Dynamics in Cislunar Environment," *71st International Astronautical Congress*, 2020.